LASER INTERFEROMETER GRAVITATIONAL WAVE OBSERVATORY
–LIGO–
CALIFORNIA INSTITUTE OF TECHNOLOGY
MASSACHUSETTS INSTITUTE OF TECHNOLOGY

Technical Note	**LIGO-T010073-00-L**	**June 22, 2001**
Geophysical Measurements Along the X Arm at LLO		
Mark Coles		

Distribution of this draft:
-

This is an internal working note
of the LIGO Project.

California Institute of Technology
LIGO Project - MS 18-34
Pasadena, CA 91125
Phone (626) 395-2129
Fax (626) 304-9834
E-mail: info@ligo.caltech.edu

Massachusetts Institute of Technology
LIGO Project - MS 20B-145
Cambridge, MA 01239
Phone (617) 253-4824
Fax (617) 253-7014
E-mail: info@ligo.mit.edu

LIGO Hanford Observatory
PO Box 1970, Mail Stop S9-02
Richland, WA 99352
Phone (509) 372-8106
Fax (509) 371-8137

LIGO Livingston Observatory
PO Box 940
Livingston, LA 70754
Phone (225) 686-3100
Fax (225) 686-7189

WWW:http//www.ligo.caltech.edu/

file D:/My/SoundSpeed/soundSpeed1.tex printed March 8th, 1999.

Geophysical Measurements Along the X Arm at LLO

Measurements of the velocity of sound for the compressional and vertical shear modes of propagation along the X-arm were made using an impulsive seismic source. The compressional wave propagation velocity is 1780 ± 80 m/sec and is independent of frequency in the 22-34 Hz region. The vertical shear wave propagation velocity varies from 230-440 meters/second over the frequency region from 4-16 Hz. The vertical shear wave mode loss quality factor, Q, varies from about 3-14 over this frequency interval. The compressional wave mode Q values vary from 3-70 over the frequency interval from 22-34 Hz. The mean values of the $1/e$ attenuation lengths for the time domain signals are 300 ± 6 meters for the vertical shear mode and about 1540 ± 50 meters for the compressional wave mode. Poisson's ratio is roughly estimated to be about 0.48. The X-arm of the interferometer appears to act as a seismic waveguide with a compressional wave cutoff frequency around 20 Hz.

1 Experimental Setup

During the summer of 2000, a linear array of Guralp CG 40T triaxial seismometers were set up along the west arm of the LLO interferometer in order to measure the seismic propagation velocity. This document summarizes the results derived from these measurements. We obtained eight Guralp CG 40T seismometers and Reftek data recorders from the IRIS PASSCAL Instrument loan center [1]. This is the same model seismometer that is used by the PEM system at each site. The seismometers were placed at 500 meter intervals along the X-arm of the interferometer on the gravel strip between the beam tube slab and the asphalt pavement near the centerline of the berm. The first seismometer was located 500 meters west of the interferometer vertex and the remaining members of the ensemble were distributed further to the west. The sampling rate of the data recorders was set at 250 samples/sec and the data were collected using the differential signal outputs from each instrument so that the seismometer sensitivity was 800 volts/meter/second. The ADC scale factor used to convert counts to volts is 7.5 volts/65536 counts. To compute velocity output, the data recorder raw ADC counts were also corrected by dividing by the recorder gain (word 120 of the SEGY data header). The timing of the data samples was corrected using the millisecond GPS offset (word 206 of the data header) *added* to the start time of the data record. (The convention of adding this value was checked for consistency with the timing synchronization command used in the alternative SAC format and found to produce identical values between the two formats.) This is a critical value that is essential in making array measurements using the Reftek recorders since the clock ticks which trigger the ADC's are not synchronized between recorders and can vary by large fractions of one second between recorders.

A simple, but effective, impulsive seismic source was made using a 2 liter plastic soda pop bottle partially filled with liquid nitrogen. A steel weight was attached to the bottle with duct tape prior to filling to insure that the bottle would not float. Once a bottle was filled approximately one-third full of liquid nitrogen and the cap was tightly secured, it was thrown into the center of the erosion control pond immediately north of the LVEA. The water depth at

this location is approximately eight feet [2]. Figure 1 indicates the location of the seismic array relative to other features on the LLO site.

When the soda bottle ruptured at the bottom of the pond, the water above it served as a reaction mass, making it possible to couple a relatively large amount of energy into the soil as a result of the explosion. Also, because the gas explosion is in water, the initial propagation through water is via a compressional wave and vertical "gravity" water wave motion. Vertical and horizontal shear modes result from the coupling at the soil-water interface at the pond boundary.

Figure 2 shows the time series data for the vertical axes of the seismometers obtained from the four seismometers closest to the pond. The seismometer serial numbers, in order of increasing distance from the source, are 7333, 7451, 7447, and 7348, located at distances from interferometer vertex of 500, 1000, 1500, and 2000 meters respectively, and 7343 which was located at 3000 meters. The decrease in amplitude of the seismic signals with increasing distance from the source is apparent in figure 2. Also visible in 7333, 7451, and 7447 are the distinct arrivals of the compressional wave signals, coupling via Poisson's ratio, into the vertical axis of each seismometer. This is followed by the later arrival of the much larger amplitude vertical shear wave signal. Seismometers 7348 and 7343 shows no obvious arrival from either the compressional or shear wave modes when viewed in the time domain on the scale of figure 2. Horizontal seismometer data was also taken at the same time, but this data was unfortunately corrupted and could not be used for this analysis. Also, three additional data recorders failed altogether and provided no useful data.

In figure 3, the arrival times of the compressional and vertical shear wave signals are plotted versus the location of each seismometer along the X-arm relative to the interferometer vertex. Arrival times were estimated simply by looking within the data at the earliest time that the seismic signal was distinguishable by eye from the preceding background. The reciprocal slopes of these lines are the propagation velocities of the two modes. The vertical shear wave propagation velocity is approximately 368 ± 11 meters/sec and the compressional wave velocity is approximately 1780 ± 80 meters/sec. This gives a distance from the explosion location to the first seismometer of 457 ± 20 meters, in agreement with the location of the pond boundary.

The amplitude data that were measured make it possible to determine how the waveforms attenuate with distance. This was estimated using the three closest seismometer signals and observing the variation in the amplitude of each mode with distance. It was expected that the energy of the seismic waves would propagate primarily along the earth's surface, so that the amplitude should diminish inversely as the square root of the distance of each seismometer from the source. Surprisingly, this turned out *not* to be the case. Figure 4 shows a semilog plot of the ratios of the maximum amplitudes for the nearest and second nearest seismometers for each mode. Also shown on the plot are the same ratios scaled by the inverse ratio of the square root of their relative distances, $(u_2/u_1) \times \sqrt{r_1/r_2}$ where u_i is the velocity signal at seismometer i and r_i is the distance of seismometer i from the source. It is obvious from the data that the signal attenuates exponentially as e^{-r_i/r_1} rather than as $e^{-r_i/r_1}/\sqrt{r_i}$. The $1/e$ attenuation lengths are 399 ± 6 meters for the shear mode and 1540 ± 50 meters for the compressional wave mode.

Why should the signals for both the shear and compressional waves decrease exponentially with distance and not as an exponential multiplied by $1/\sqrt{r}$? One would expect that the signals spread out circularly on the earth's surface so that their amplitudes should decrease as $f(r)/\sqrt{r}$ to conserve energy. Both arms were constructed from compacted and stabilized fill dirt. The berm is also loaded by the beam tube slab, beam tube, and enclosure. However, the berm is likely to be stiffer than the surrounding soil. Because the dynamic properties of the berm are different from that of the surrounding undisturbed soil, this creates an acoustic impedance boundary. This might allow the berms to act as wave guides, confining acoustic energy within the arms so that the signals attenuate only exponentially. If this is the case, this could increase the coherence

in the seismically induced motion of the end and input test masses of the interferometer.

2 Poisson's Ratio

Using the mean values of the propagation velocities for the compressional and shear waves, one can crudely estimate Poisson's ratio for the berm. The compressional wave velocity for an isotropic medium is $v_c = \sqrt{K/\rho}$, where K is the bulk modulus and ρ is the density. Similarly, *if* the vertical shear wave velocity is $v_s = \sqrt{\mu/\rho}$, where μ is the shear modulus (and this *may not* be correct since the berm is a complex structure while these formulae are for isotropic media), then Poisson's ratio σ is given by

$$\frac{K}{\mu} = \frac{2(1+\sigma)}{3(1-2\sigma)}$$

Using $v_c = 1780$ meters/second and $v_s = 379$ meters/second, $\sigma = 0.48$. For comparison, an incompressible fluid has $\sigma = 0.5$ while many metals have values around 0.3. Woodward-Clyde[3], on the basis of static tests, had previously recommended to LIGO that $\sigma = 0.4$ be used for in-situ soil calculations on the LIGO site.

3 Spectral Analysis of the Seismometer Signals

It is interesting, for many studies of the interferometer's sensitivity to seismic motion, to see what can be learned by looking at the measured data in the frequency domain. The dependence of the propagation velocity and attenuation length on frequency for each mode have been investigated using this data. The MATLAB routine **specgram** was used to make time versus frequency plots for each of the data series shown in figure 2. **Specgram** computes the FFT for a window of data which slides over the time series data. Using the output of **specgram**, the velocity data were converted to displacement power spectral densities and the log of the magnitude of the displacement spectral density in meters/$\sqrt{\text{Hz}}$ is plotted in figures 5-9. To make each spectrogram, 256 element time records were successively Fourier analyzed using a Hanning window and an overlap of 252 points. The arrivals of the acoustic signals are easily observable as vertical bands in the spectrograms. The time axis in each figure is in seconds after the hour measured using the GPS antennae within each data recorder corrected for the clock slough between recorders.

The attenuation of the shear mode as a function of frequency was estimated from the maximum amplitude of the shear arrival at each frequency. The measurements were made only in the frequency region from 5-17 Hz where the shear and compressional wave signals could easily be discriminated from each other. The times at which the maximum occured in various frequency bands at successive interferometers were used to determine the velocity as a function of frequency. These data are shown in table 1. Because the shear waveforms diminish with distance and the pulses sometimes spread out in time, the measurements could not be made at every frequency. Only data are included where a well shaped pulse is clearly visible on two seismometers. The uncertainties listed in the table are estimates of the accuracy with which the arrival time and amplitude of the wave could be determined from the seismogram. Figures 10 and 11 show the amplitude ratio and propagation velocity as a function of frequency. Combining the ratio of the amplitude spectral densities and attenuations allows the figure of merit,

$$Q(f) = -\frac{2rf}{v}\ln(\frac{x_{\text{far}}}{x_{\text{near}}})$$

the number of cycles required for the energy at a particular frequency to fall to $1/e$, to be calculated. This is shown in figure 12.

Note the rather surprising peak in $Q(f)$ which occurs around 9 Hz. Although it has large measurement uncertainties, one possible explanation for this peak is that the wavelength at this frequency (approximately 32 ± 3 meters) is close to the spacing between the beam tube fixed supports. This or some other longitudinal spatial impedance periodicity could create variations in propagation velocity and attenuation with frequency similar to that observed. This lends additional support to the idea that the interferometer berms act as waveguides.

The compressional wave signal was similarly analyzed. It is interesting that the compressional wave arrival at the most distant seismometer is easily apparent in the spectrogram of figure 9, even though there is no indication of this in the time domain data shown in figure 2. It is also apparent from the spectrograms of figures 5-9 that the compressional wave velocity has very little frequency dependence over the region from 20-40 Hz since the vertical band associated with the arrival of this mode remains vertical over the 3000 meter distance to the most distant seismometer. A third feature visible in the spectrograms is that the compressional wave signal propagates much further in the 20-30 Hz band than it does at lower frequencies. This is especially obvious in figure 9. There appears to be a frequency cutoff below around 20 Hz, which is additional support for the notion that the berm acts as a waveguide. Interestingly, the cutoff frquency for a two dimensional waveguide is equal to the frequency at which one-half wavelength equals the transverse dimension of the waveguide. For the compressional wave, using a cutoff frequency of 20 Hz and a propagation velocity of 1780 meters/second gives a transverse dimension for the waveguide of 44.5 meters or 146 feet. This corresponds almost precisely to the 150 foot width of the disturbed section of soil along the X arm of the interferometer. The corresponding shear wave cutoff frequency is therefore estimated to be less than 2.7 Hz assuming a waveguide transverse dimension of 150 feet and a propagation velocity of less than 250 meters/second (from figure 10).

The attenuation of the compressional wave signal does exhibit a frequency dependence, and the resulting $Q(f)$ is shown in figure 13 using the data from table 2. It is somewhat difficult to discern the amplitudes of the compressional wave signals at lower frequencies. In the nearest detector to the source, the waveforms overlap with the shear wave, and as they propagate farther away, the peaks become less well defined. In the 20-25 Hz frequency region it is very difficult, using the complicated time versus frequency data that result from the spectrogram computation, to compare the maximum amplitude at each frequency for different seismometers. For example, figures 14 and 15 show the time variation of the spectral density for some representative frequencies that illustrate simple and complex waveforms. The 28.3 Hz arrival of the compressional wave is easy to distinguish in the near detector (7333) and in the detector 500 meters further away (7451). The pulse shape looks about the same but decreases in amplitude as the wave moves away from the source. On the other hand, the 23.4 Hz waveform changes shape as it propagates, so comparing peak amplitudes is probably not a good way to measure the attenuation since the duration of the pulse gets wider at that frequency. At 18.6 Hz, the compressional wave signal is strongly attenuated in seismometer 7451. The data within the limited frequency range from 20-25 Hz exhibit very little attenuation. Since the measured attenuation is so small, uncertainties in how the amplitude might be influenced by changes in the pulse shape make it impossible to estimate the attenuation within this range with any degree of confidence. Overall, in the 22-34 Hz band, the data do seem to indicate some periodicity in the compressional wave attenuation, although the wavelengths of the peaks do not correspond to any obvious structural periodicity within the berm.

4 Conclusion

The interferometer arms appear to act as crude waveguides in which seismic motion can propagate with surprisingly little attenuation above a cutoff frequency for each mode. The strongest

evidence for this comes from the exponential dependence of the attenuation on distance from the source and the apparent cutoff frequency for compressional waves of around 20 Hz. It should be worthwhile to look for correlations in the horizontal motion of the seismometers along the direction of each interferometer arm at frequencies as high as 20-30 Hz and the data from seismometer 7343, 3000 meters from the source demonstrates this possibility. For example, at 28 Hz, the wavelength of the compressional wave is approximately 1780 meters/sec/28Hz = 55 meters. Comparing only the spectrograms of seismometers 7333 and 7343 and looking at the peak amplitude of the compressional arrival at 28.3 Hz gives a Q of around 50, so the $1/e$ length should be possibly as high as 2.8 KM. The Y-arm berm at LLO has a cross section that is twice as wide as the X-arm, so the cutoff frequency in this direction for compressional waves is expected to be around 10 Hz.

The mechanical properties of the berm are different from the surrounding soil and therefore the sound speed and attenuation within the berm are probably somewhat different from the surrounding area. Use of the measurements reported here to estimate the degree of seismic coupling of the interferometer to road noise and other distant noise sources should be done with some caution. One would expect that in the general area the soil should have lower shear and compressional moduli, but also possibly lower density and a different relationship between attenuation and source distance.

Acknowledgments

The setup of the seismometers along the X-arm and the collection of the data using the Reftek data loggers was done by Kevin Tubbs, a student from Southern University who was a SURF Fellow at LLO during the summer of 2000. The author wishes to thank him for his assistance with this project.

References

1. The IRIS PASSCAL Instrument Center is located at the New Mexico Institute of Technology and is supported by the National Science Foundation. Further details about the center can be found at **http://www.passcal.nmt.edu/**.
2. The explosive seismic sources require some caution. We found that the 2-liter bottles filled one third full of liquid nitrogen require about 2 minutes to burst in air once the cap is tightly sealed, but once they are thrown into water they burst about five seconds after submersion. It is therefore important that they be properly weighted so that they quickly sink to the bottom of the erosion control pond to protect experimenters from debris. We took the additional safety precautions of moving well clear of the pond immediately after the sources were thrown into the pond.
3. Geotechnical Investigation of the LIGO Site - Final Report. Woodward-Clyde Consultants, January 1995. WCC File 93B107C, page 11. They report a typical shear wave velocity of 700 feet/second (214 meters/second), with values ranging from 550-850 feet/second (168-259 meters/second) over the various soil types and conditions found on the LLO site. Since the berm has been compacted and stabilized, one might expect somewhat faster sound speeds than the Woodward-Clyde measurements in undisturbed soil, and this seems to be the case. Woodward-Clyde's measurements of Poisson's ratio range from 0.2-0.5, with the highest value appropriate for water saturated clays and the lowest values for the sandy/silty clays (typically the top two feet of formation underlaying the thin veneer of top soil). They recommend using $\sigma = 0.4$ as a typical value for soils on-site, which means that the soil will support more shear than the berm measurements in this report indicate.

Table 1: Vertical shear mode amplitudes and arrival times versus frequency

	Seismometer 7333		Seismometer 7451	
frequency	arrival time	log10(amplitude)	arrival time	log10(amplitude)
4.88	517.50 ± 0.02	-6.38 ± 0.02	519.5 ± 0.1	-7.56 ± 0.03
5.86	517.87 ± 0.02	-6.087 ± 0.005	519.0 ± 0.1	-7.56 ± 0.03
6.85	517.96 ± 0.02	-5.82 ± 0.02	519.3 ± 0.1	-6.77 ± 0.03
7.81	518.1 ± 0.1	-5.93 ± 0.02	519.55 ± 0.05	-6.50 ± 0.03
8.79	517.8 ± 0.1	-6.5 ± 0.2	519.60 ± 0.05	-6.54 ± 0.03
9.77	517.4 ± 0.1	-6.14 ± 0.03	519.4 ± 0.05	-6.89 ± 0.03
10.70	517.5 ± 0.1	-6.1 ± 0.1	519.7 ± 0.05	-7.3 ± 0.1
11.70	517.5 ± 0.1	-6.4 ± 0.2	519.5 ± 0.1	-7.55 ± 0.03
12.70	517.4 ± 0.1	-6.82 ± 0.03	519.65 ± 0.05	-8.06 ± 0.03
13.70	517.32 ± 0.03	-7.07 ± 0.2	518.95 ± 0.05	-8.05 ± 0.03
14.60	517.28 ± 0.03	-7.16 ± 0.03	519.1 ± 0.1	-8.03 ± 0.03
15.60	517.35 ± 0.03	-7.2 ± 0.1	519.2 ± 0.1	-8.2 ± 0.1
16.60	517.5 ± 0.1	-7.13 ± 0.03	519.35 ± 0.05	-8.5 ± 0.1

Table 2: Compressional mode amplitudes and arrival times versus frequency

	Seismometer 7333		Seismometer 7451	
frequency	arrival time	log10(amplitude)	arrival time	log10(amplitude)
21.5	516.4 ± 0.01	-8.03 ± 0.01	516.70 ± 0.01	-8.35 ± 0.02
22.5	516.60 ± 0.05	-8.12 ± 0.02	516.7 ± 0.1	-8.23 ± 0.03
24.4	516.30 ± 0.01	-8.33 ± 0.02	516.62 ± 0.03	-8.02 ± 0.02
28.3	516.40 ± 0.01	-7.92 ± 0.01	516.65 ± 0.01	-7.97 ± 0.02
29.3	516.35 ± 0.01	-7.96 ± 0.01	516.70 ± 0.01	-8.03 ± 0.02
30.3	516.35 ± 0.01	-8.10 ± 0.01	516.75 ± 0.01	-8.25 ± 0.02
34.2	516.20 ± 0.01	-8.9 ± 0.1	516.5 ± 0.01	-9.25 ± 0.02

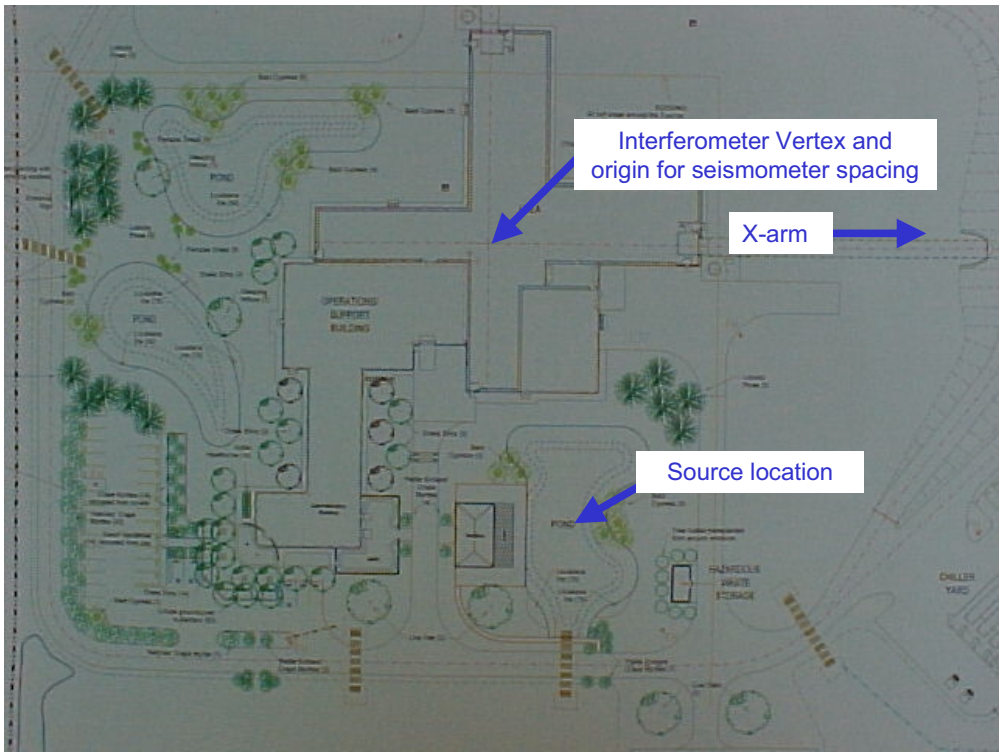

Figure 1: Physical layout of the seismometers and erosion control pond at LLO

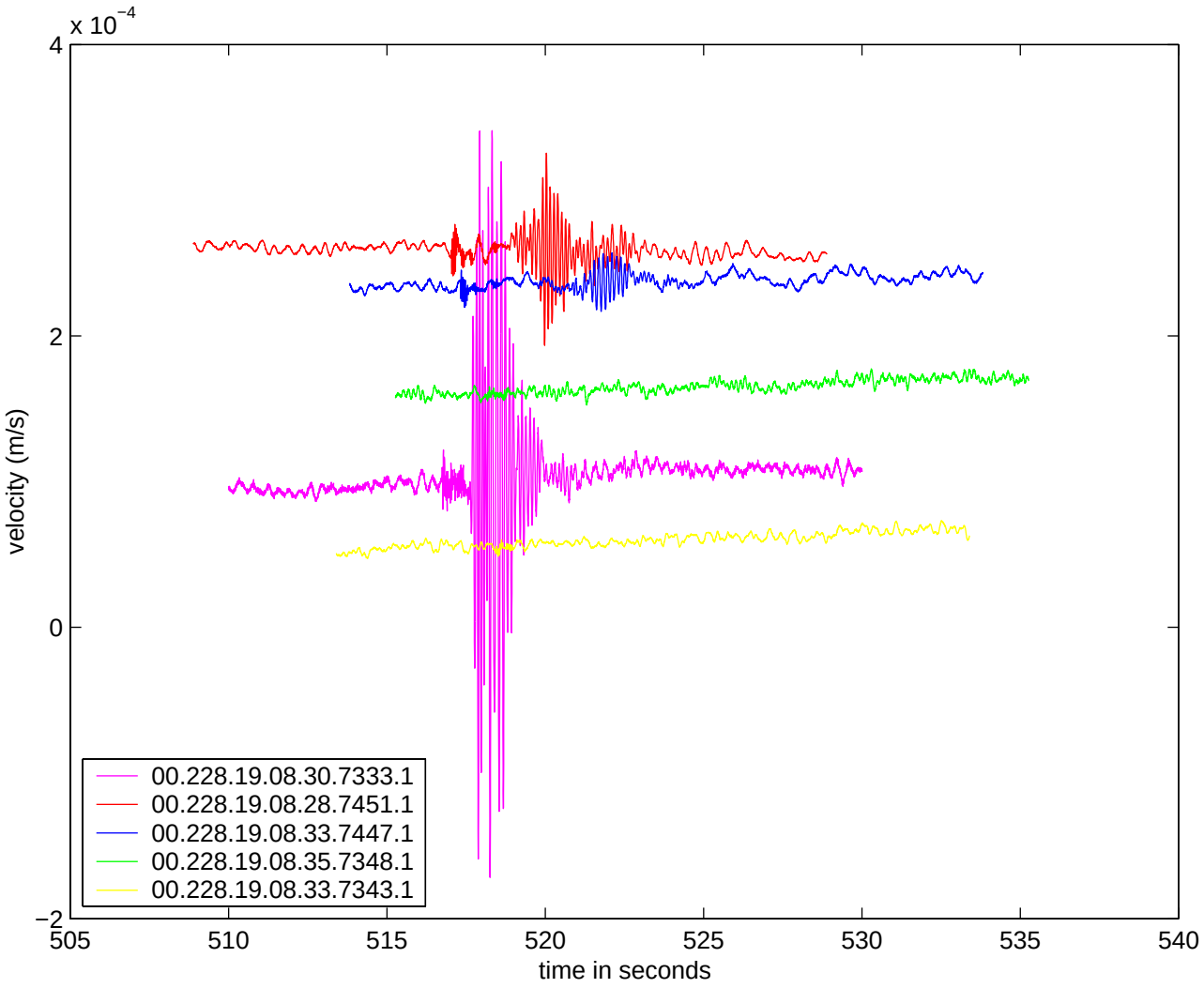

Figure 2: Time series for the vertical axes of the four closest seismometers

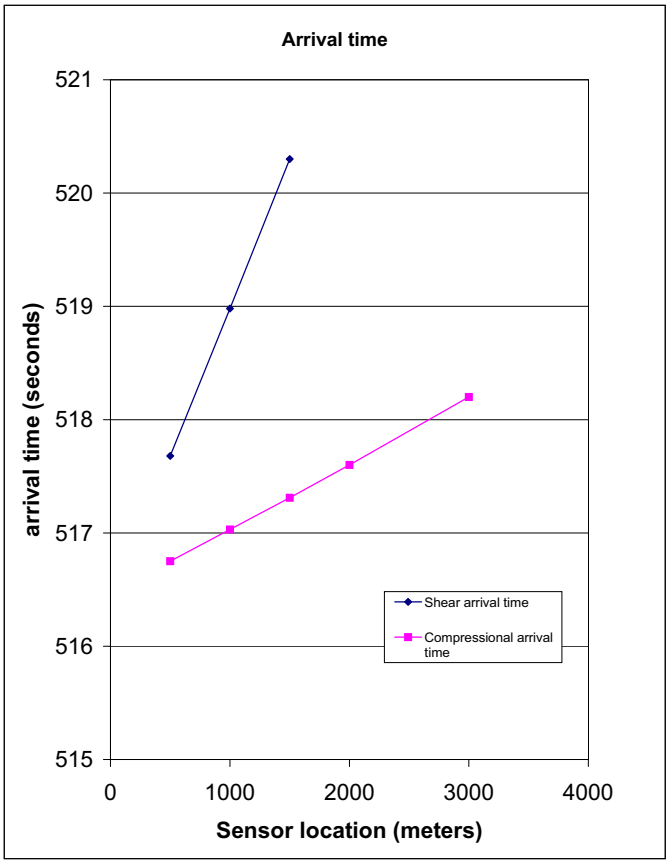

Figure 3: Arrival times of the compressional and vertical shear waves at each seismometer

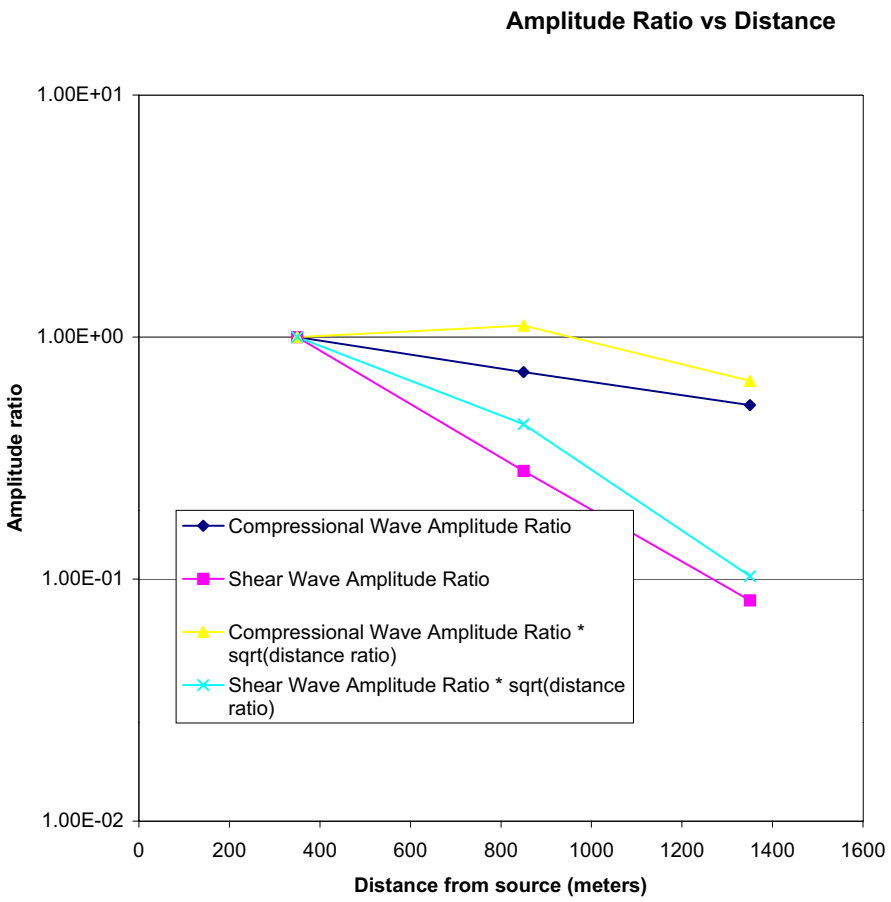

Figure 4: Amplitude ratios of the seismometer signals relative to the signals measured at the seismometer closest to the source.

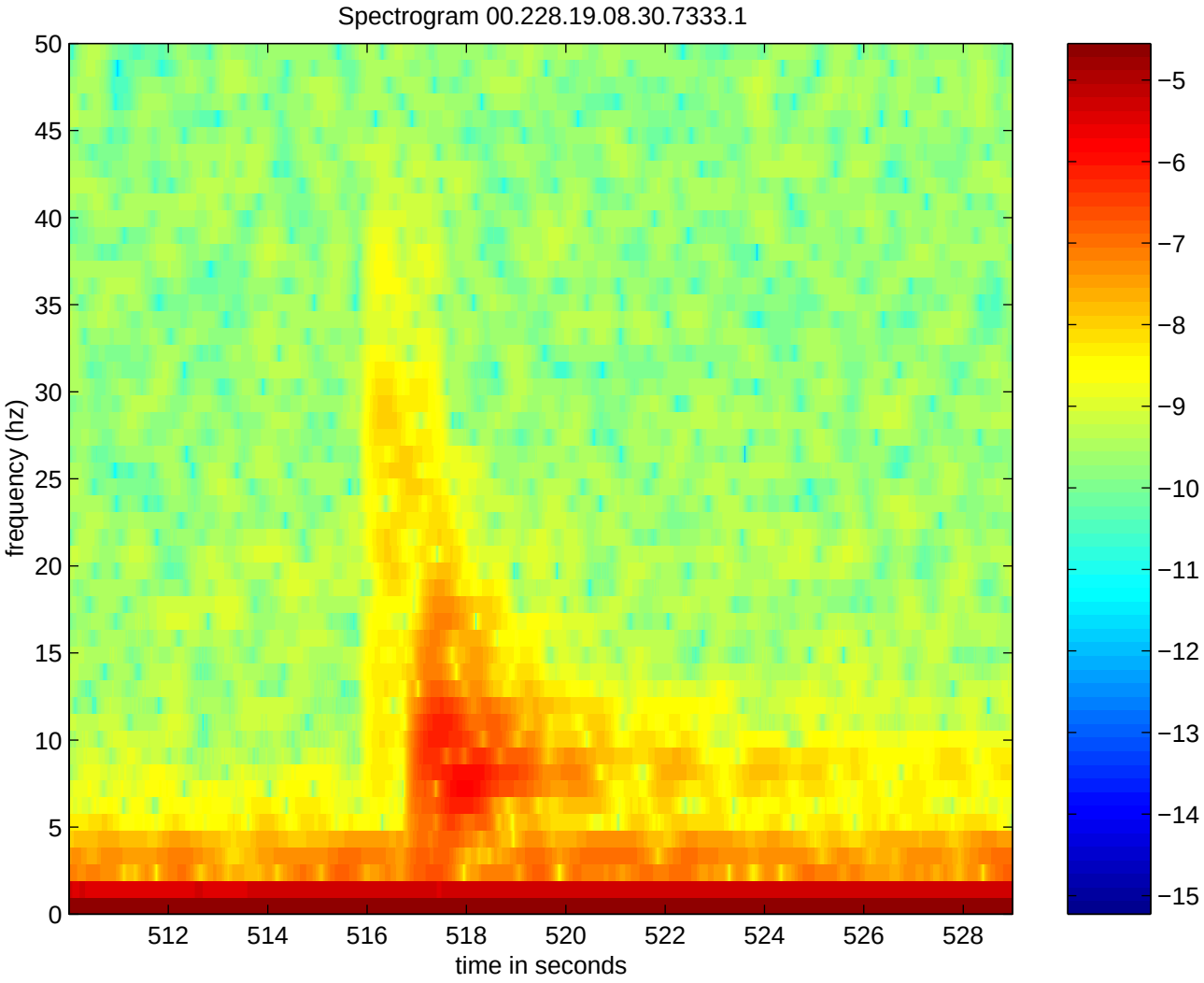

Figure 5: Spectrogram of seismometer 7333. The plot shows the magnitude of the displacement spectral density versus time. 7333 is the seismometer closest to the source, 500 meters along the X-arm.

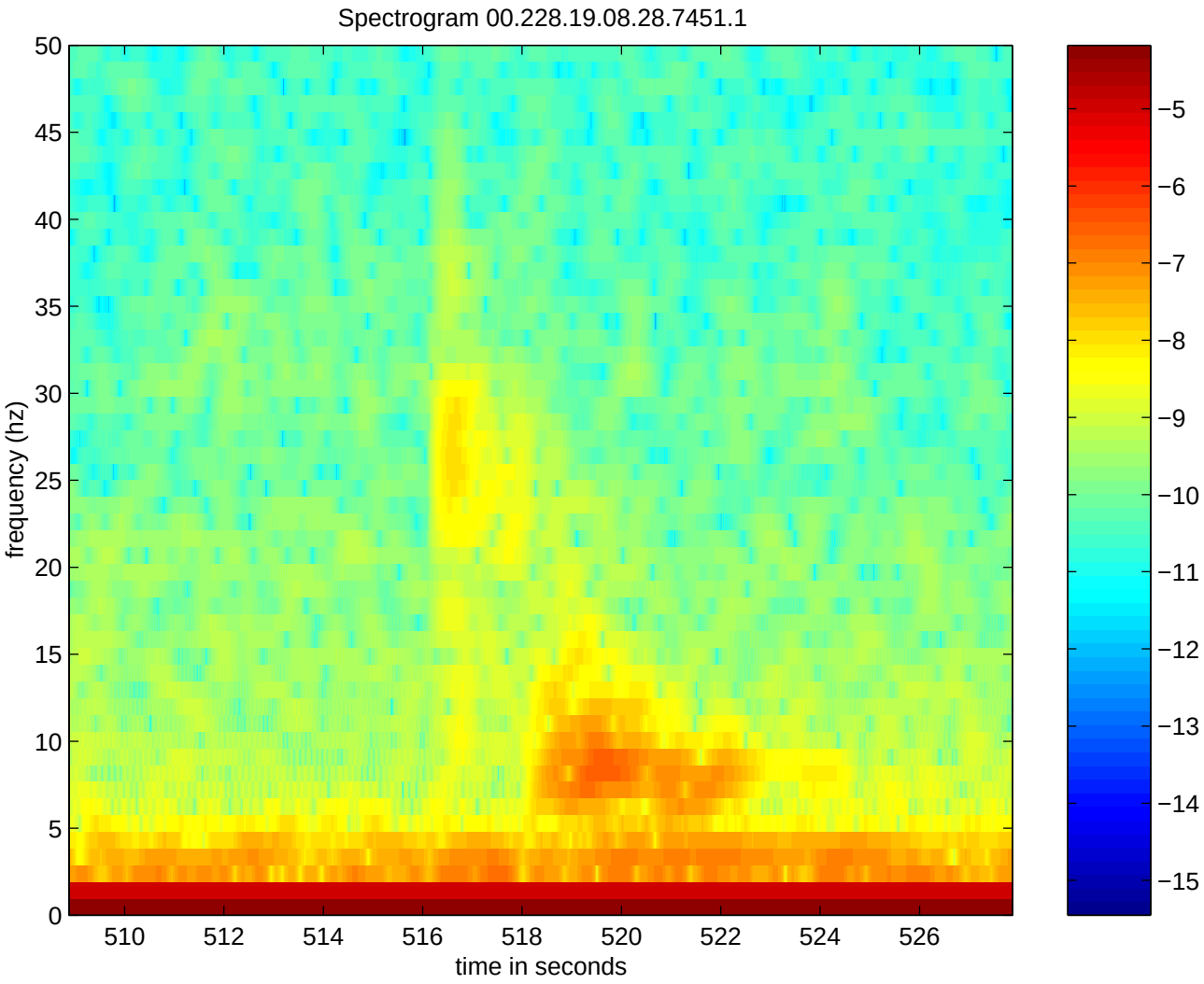

Figure 6: Spectrogram of seismometer 7451. The plot shows the magnitude of the displacement spectral density versus time. 7451 is the second closest seismometer to the source, 1000 meters along the X-arm.

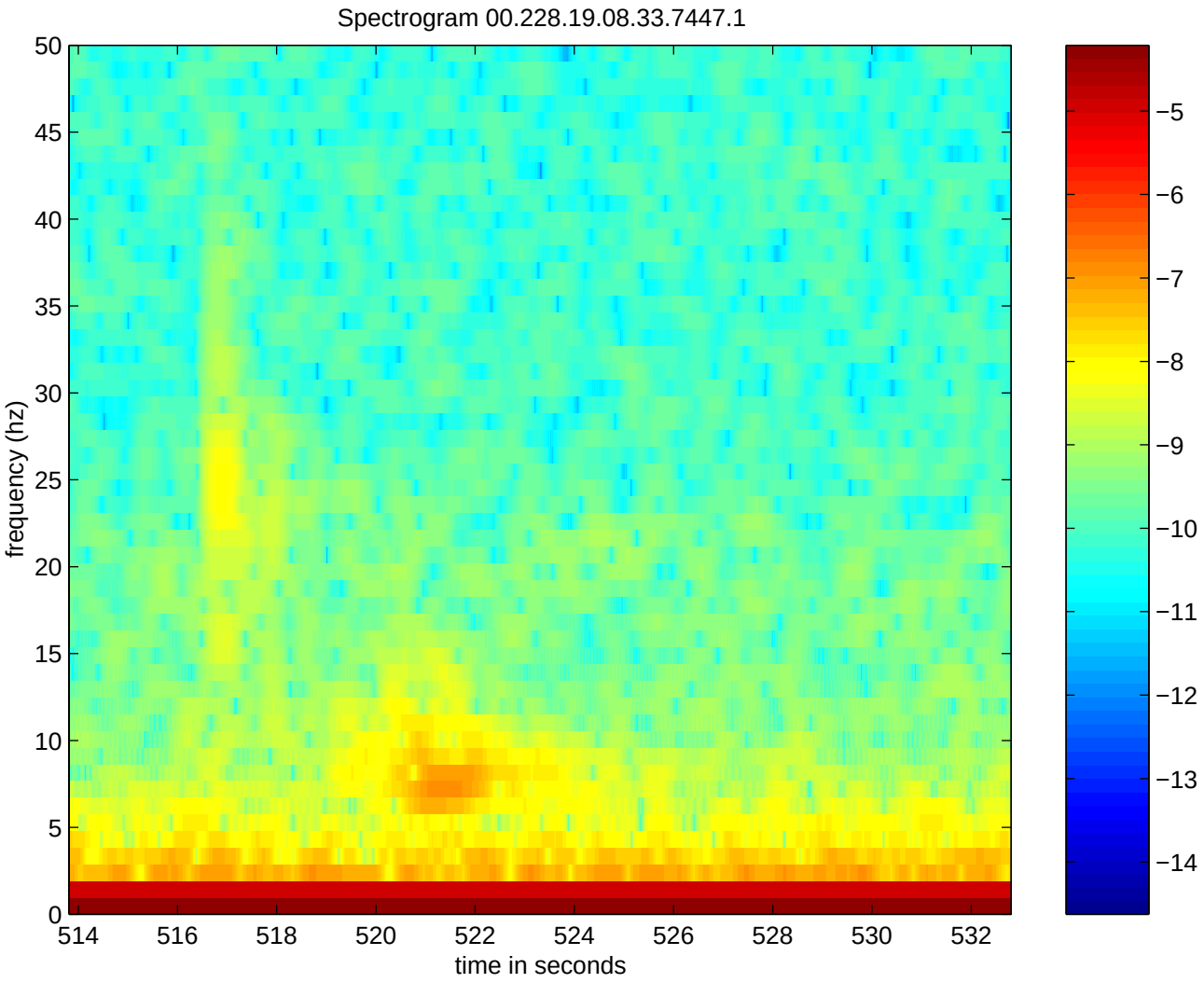

Figure 7: Spectrogram of seismometer 7447. The plot shows the magnitude of the displacement spectral density versus time. 7447 is the third closest seismometer to the source, 1500 meters along the X-arm.

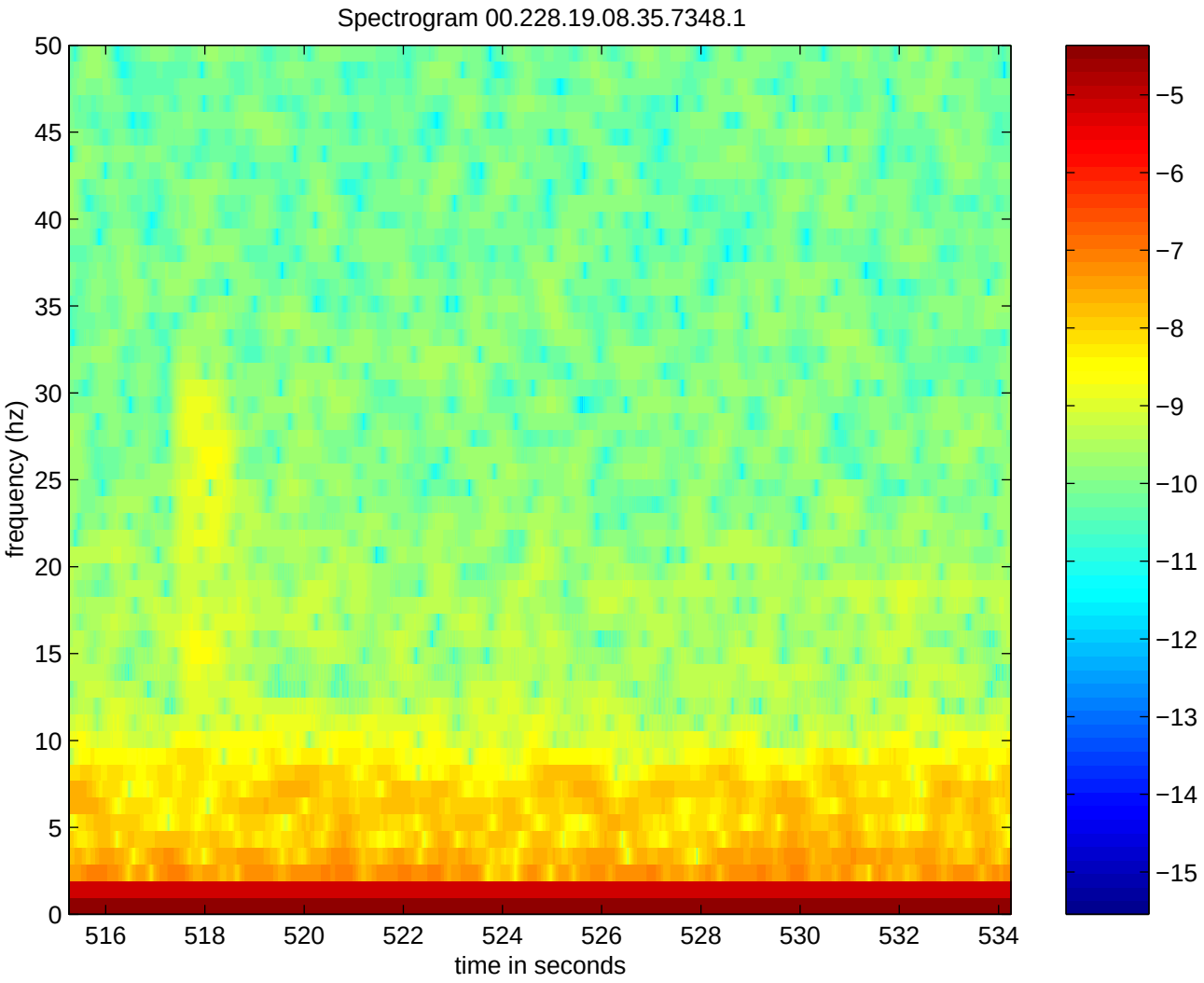

Figure 8: Spectrogram of seismometer 7348. The plot shows the magnitude of the displacement spectral density versus time. 7348 is located 2000 meters along the X-arm.

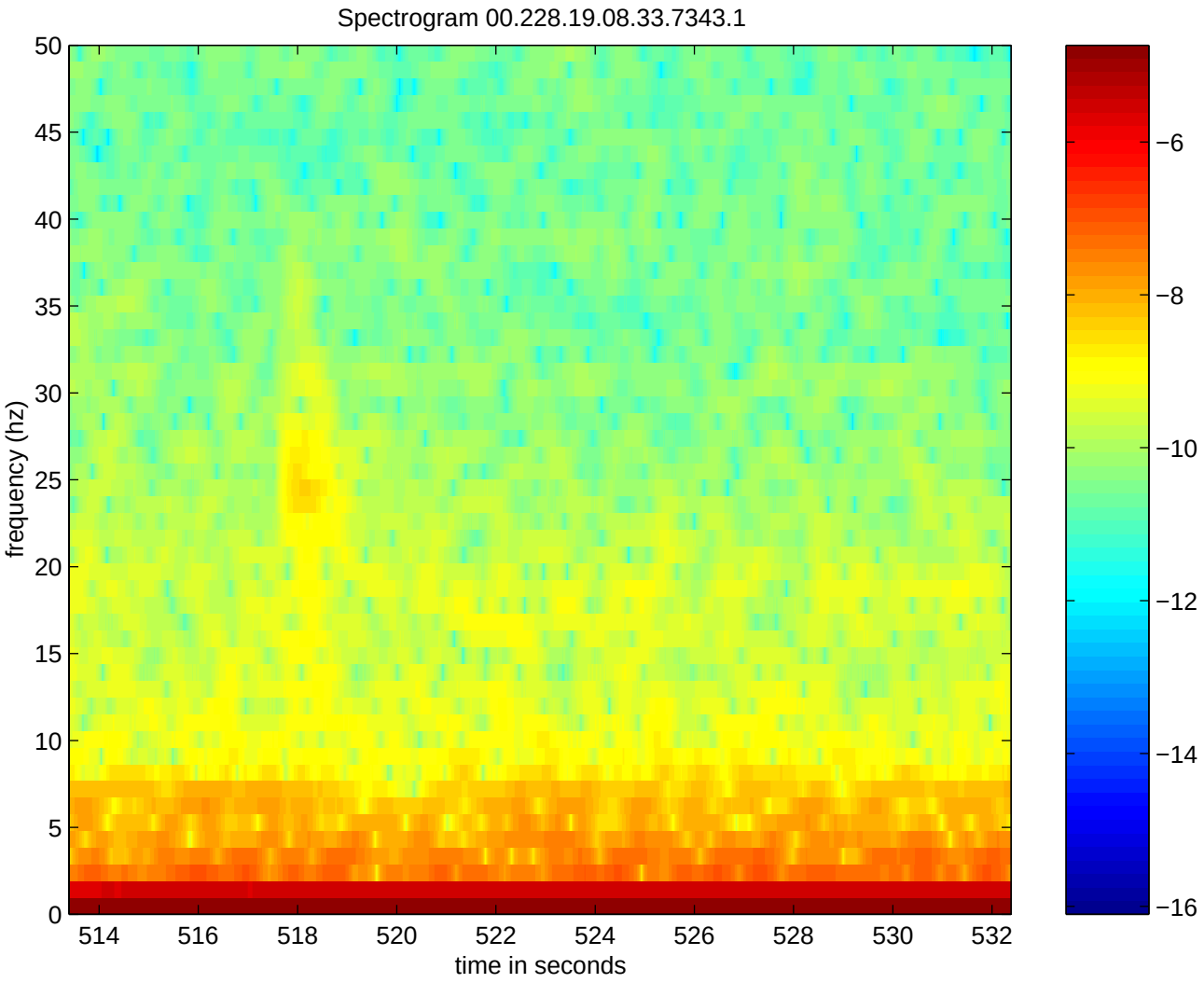

Figure 9: Spectrogram of seismometer 7343. The plot shows the magnitude of the displacement spectral density versus time. 7343 is the most distant seismometer from the source, 3000 meters along the X-arm.

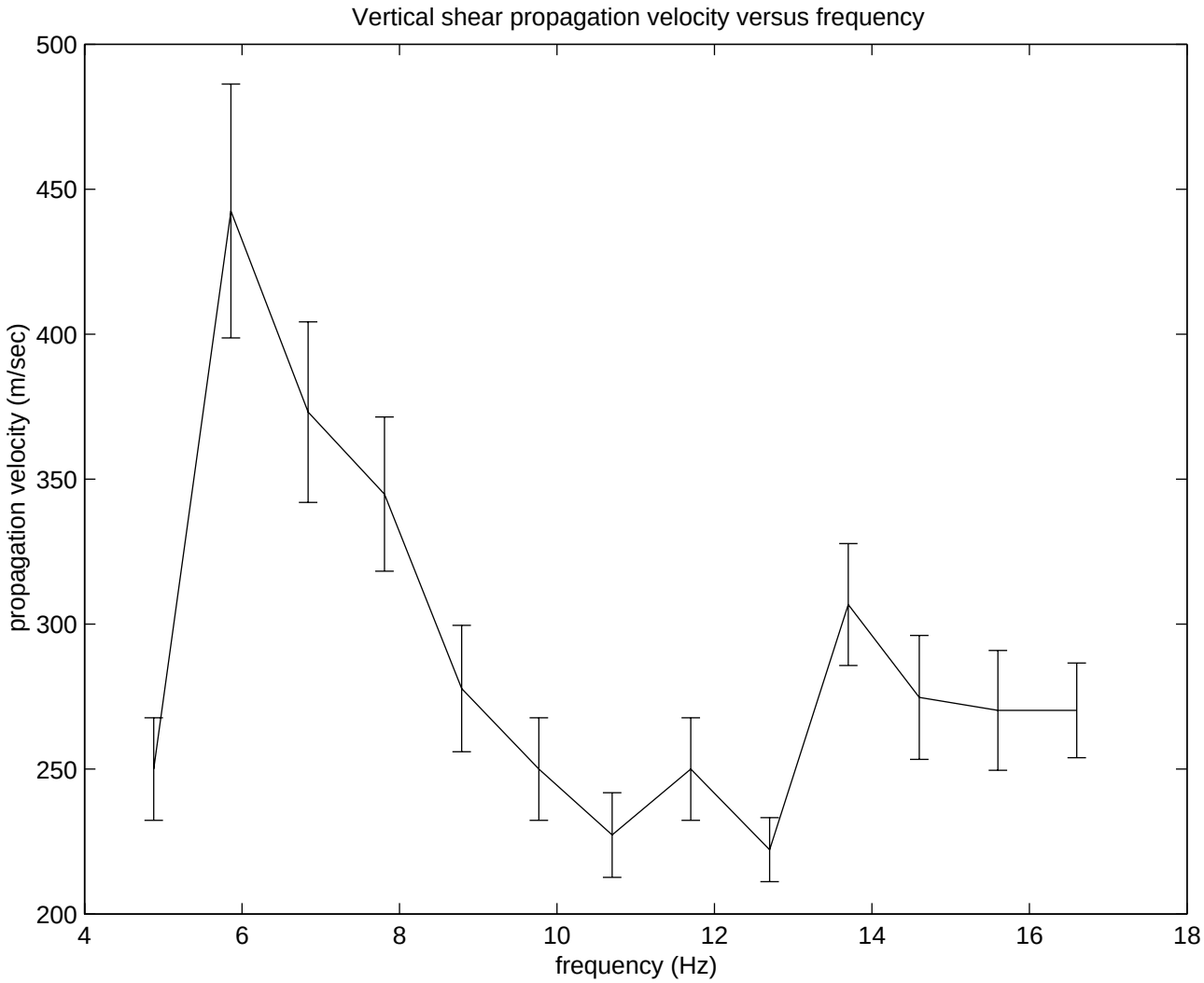

Figure 10: Ratio of the peak amplitudes of the two closest seismometers.

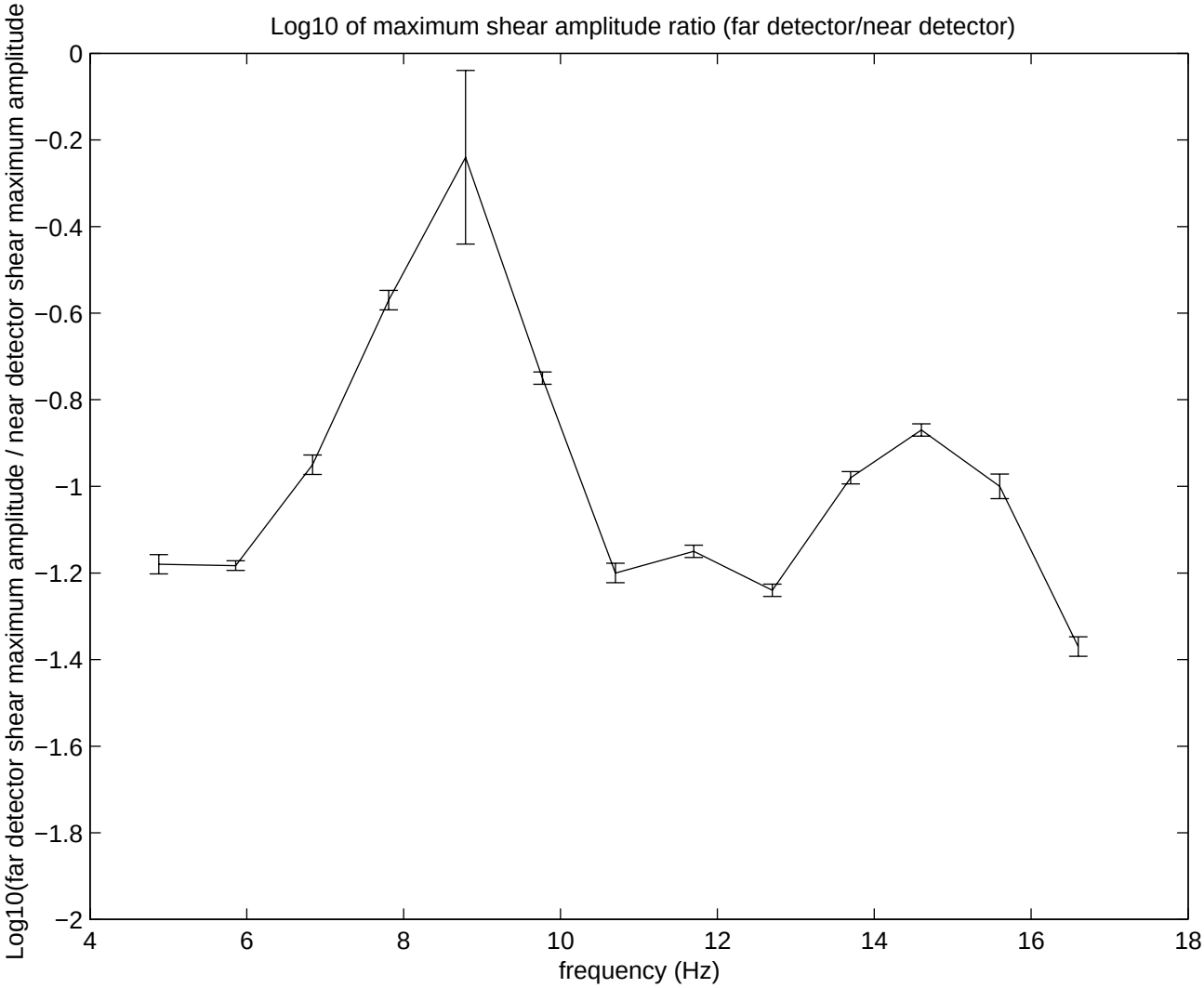

Figure 11: Shear velocity as a function of frequency.

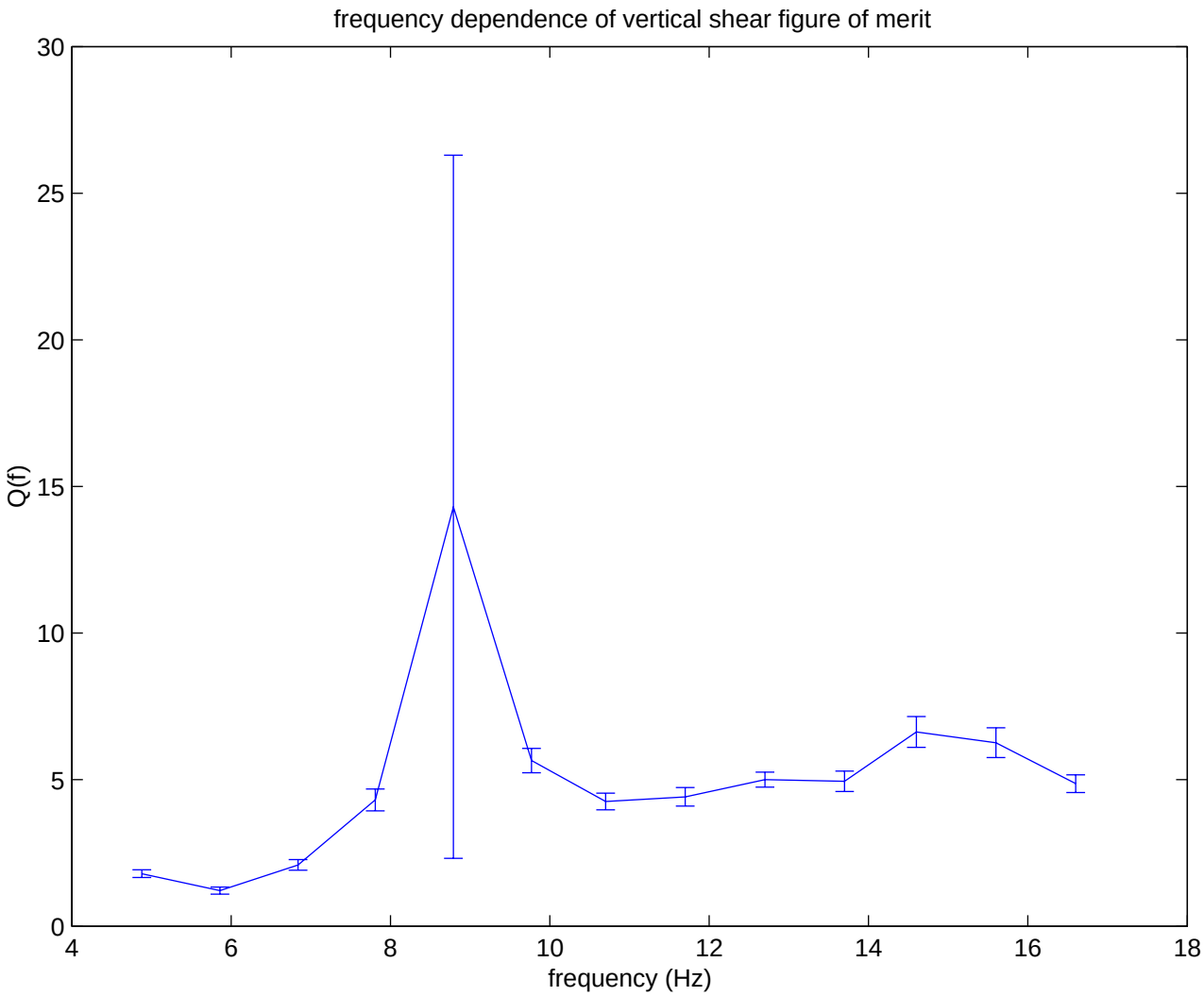

Figure 12: Figure of merit as a function of frequency.

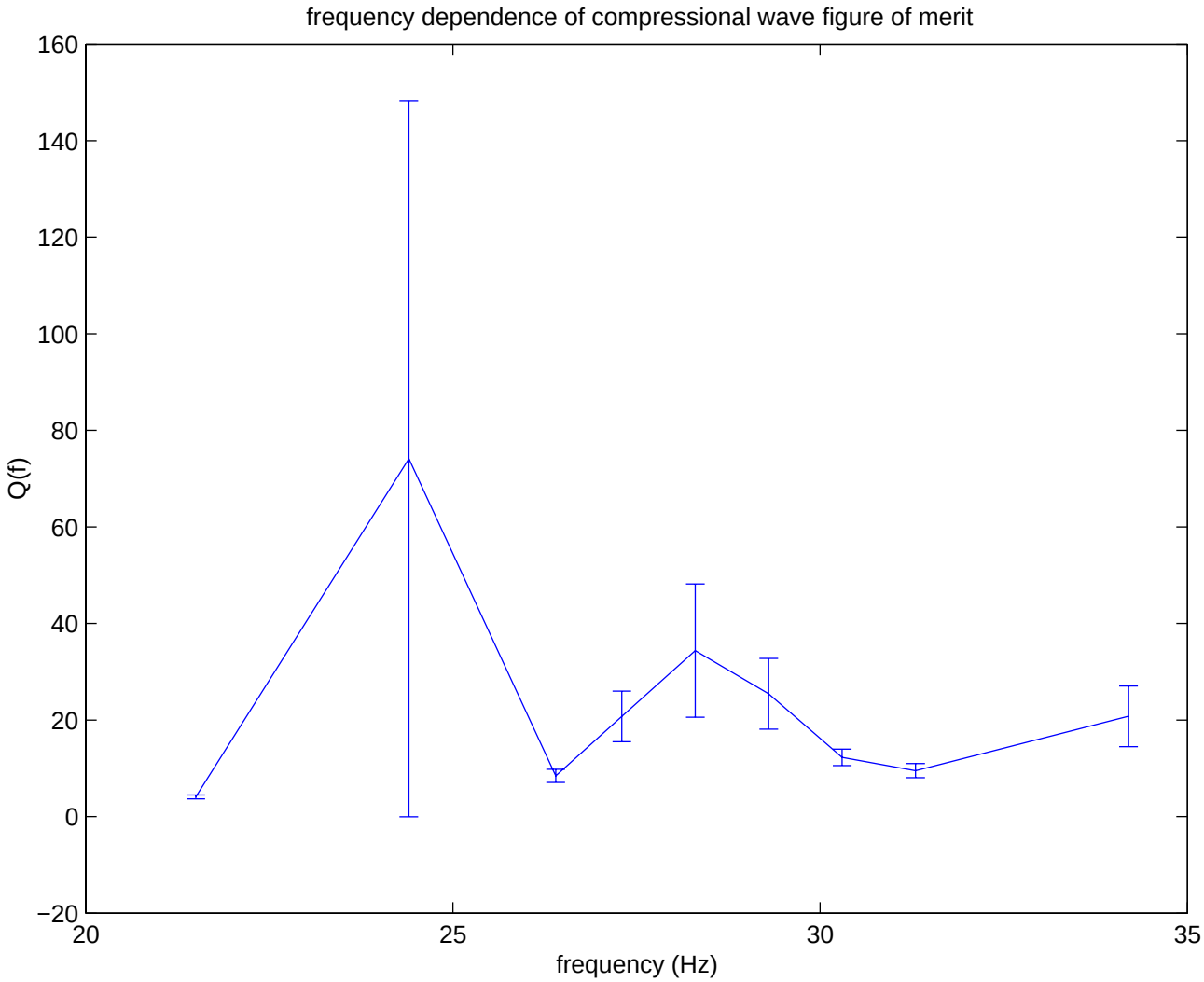

Figure 13: Figure of merit for compressional wave as a function of frequency.

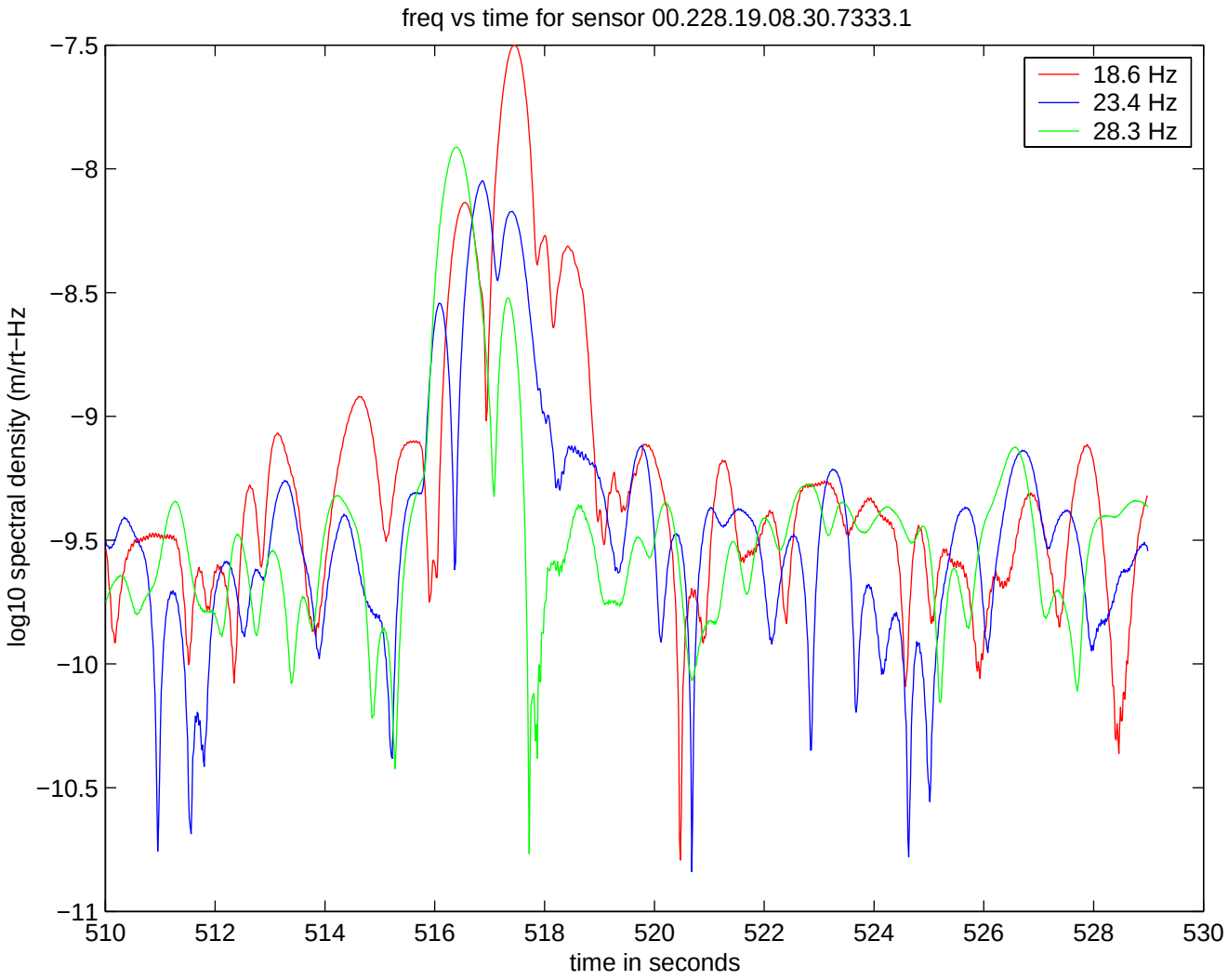

Figure 14: Amplitude versus frequency for seismometer 7333. The peaks around 517 seconds are the arrivals of the compressional wave signal.

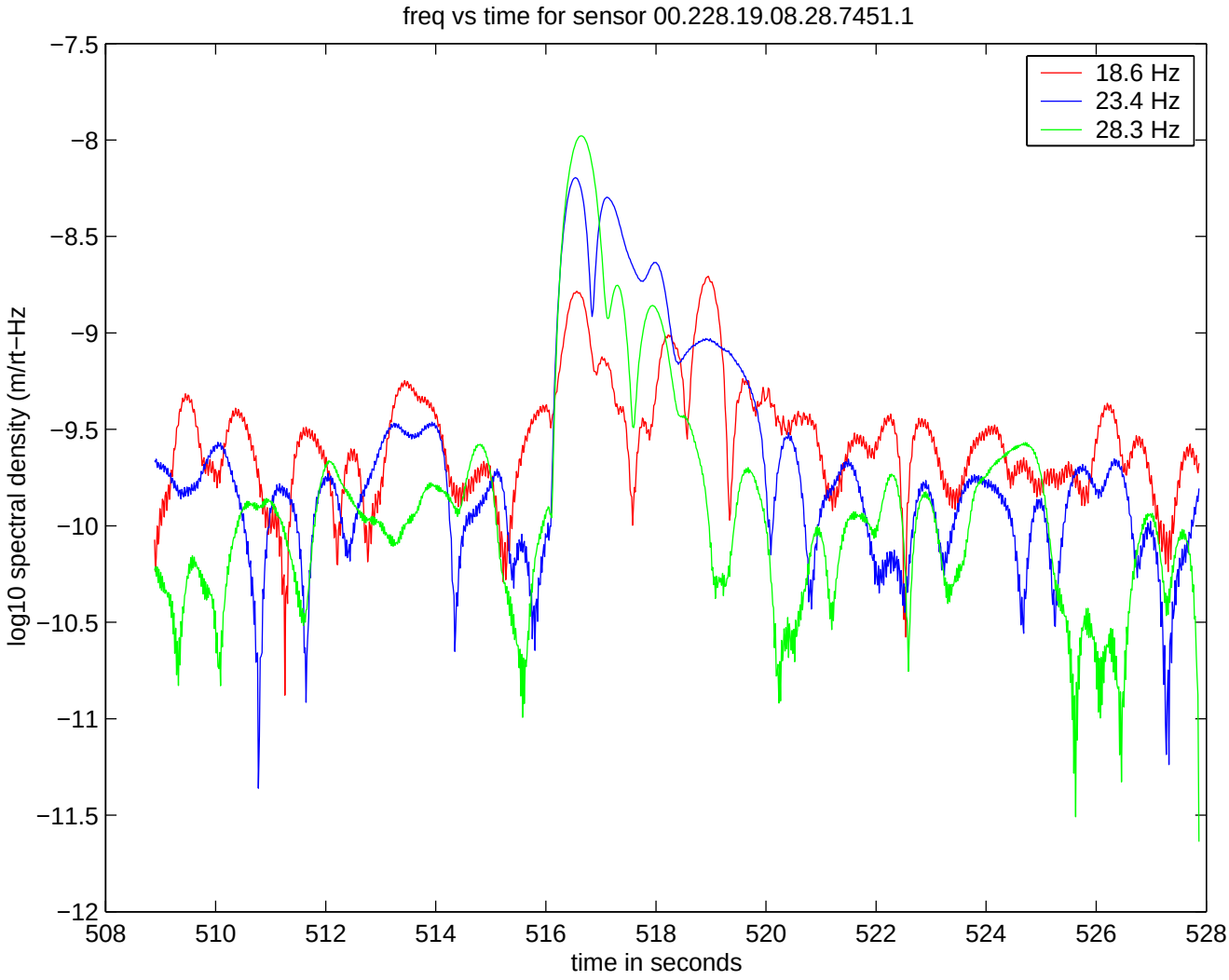

Figure 15: Amplitude versus frequency for seismometer 7451. The peaks around 517 seconds are the arrivals of the compressional wave signal. Note the strong attenuation of the signal at 18.6 Hz relative to the same frequency in figure 14.